Theor Appl Climatol (2015) 121:529–544
DOI 10.1007/s00704-014-1251-7

ORIGINAL PAPER

The impact of forest architecture parameterization on GPP simulations

Ana Firanj · Branislava Lalic · Zorica Podrascanin

Received: 28 January 2014 / Accepted: 6 August 2014 / Published online: 20 August 2014

Abstract The presence of a forest strongly affects ecosystem fluxes by acting as a source or sink of mass and energy. The objective of this study was to investigate the influence of the vertical forest heterogeneity parameterization on gross primary production (GPP) simulations. To introduce a heterogeneity effect, a new method for the upscaling of the leaf level GPP is proposed. This upscaling method is based on the relationship between the leaf area index (*LAI*) and the leaf area density (*LAD*) profiles and the standard sun/shade leaf separation method. The effect of the crown shape and foliage distribution parameterization on the simulated GPP is confirmed in a comparison study between the proposed method and the standard sun/shade upscaling method. The observed values used in the comparison study are assimilated during the vegetation period on three distinguished forest eddy-covariance (EC) measurement sites chosen for the diversity of their morphological characteristics. The obtained results show (a) the sensitivity of the simulated GPP to the leaf area density profile, (b) the capability of the proposed scaling method to calculate the contribution of the different canopy layers to the entire canopy GPP, and (c) a better agreement with the observations of the simulated GPP with the proposed upscaling method compared with the standard sun/shade method.

A. Firanj (✉) · Z. Podrascanin
Faculty of Sciences, Department of Physics, University of Novi Sad, Dositej Obradovic Sq. 4, Novi Sad 21000, Serbia
e-mail: ana.firanj@df.uns.ac.rs

B. Lalic
Faculty of Agriculture, Department for Field and Vegetable Crops, University of Novi Sad, Dositej Obradovic Sq. 8, Novi Sad 21000, Serbia

1 Introduction

Forests play an important role in the terrestrial carbon cycle because they are major reserves of terrestrial carbon and major components of the global photosynthetic accumulation of carbon, also known as the gross primary production (GPP) (Malhi et al. 1999; Pan et al. 2011). Studies have shown that a physical model of tall vegetation with defined morphological, kinematic, aerodynamic, and thermal characteristics has a strong impact on the accuracy of the parameterization of all of the surface vertical fluxes (Ellsworth and Reich 1993; Mix et al. 1994; Zeng and Takahashi 2000). Therefore, a detailed description of the forest structure in atmospheric and environmental models of different spatial and time scales can result in a better estimation of GPP, energy, and momentum exchange (Sprintsin et al. 2012). The part of the numerical weather prediction model or climate model responsible for parameterization of the processes describing land-air interaction is the soil-vegetation-atmosphere transfer (SVAT) scheme.

Traditionally, the GPP of a forest canopy has been calculated as the photosynthesis rate per unit of leaf surface, which is then upscaled to the canopy level. A biochemical model that became the standard for quantifying the leaf level carbon assimilation was developed by Farquhar et al. (1980) and was later expanded by von Caemmerer and Farquhar (1981) and Collatz et al. (1991, 1992). This model is based on the realistic description of two photosynthetic processes: the Rubisco-limited rate of ribulose bisphosphate (RuBP) carboxylation and the electron transport-limited rate of RuBP regeneration. Gross photosynthesis (A) is determined by the most limiting photosynthetic process. To predict the photosynthetic rate from the external carbon dioxide (CO_2) concentration, Farquhar's model requires coupling with a stomatal conductance model. The Jarvis (Jarvis 1976) or Ball-Berry (Ball et al. 1987) types of stomatal conductance/resistance models are often used.

The accuracy of the biophysical model depends on the upscaling method used to transfer information from the leaf level to the entire canopy and ecosystem (Schaefer et al. 2012). The upscaling method is always a product of the parameterization of the canopy architecture. The model description of the canopy structure is used in a simplified form and represented as, for example, the "big-leaf" (Sellers et al. 1997a) model, especially in the SVAT models developed for numerical weather prediction and climate models. This approach is based on an assumption of the horizontally and vertically homogeneous canopy in which the vertical profile of the absorbed irradiance is described with the Lambert-Beer's law relationship. Assuming that the distribution of the photosynthetic capacity among the leaves in a canopy is proportional to the profile of the absorbed irradiance, then the GPP calculated for a single leaf at the top of the canopy can be upscaled to the entire canopy.

The development of more sophisticated measurements has raised questions about the physical accuracy of the big-leaf upscaling method (Harley and Baldocchi 1995; Leuning et al. 1995; de Pury and Farquhar 1997; Jarvis 1995; Mercado et al. 2006; Sprintsin et al. 2012). Observations have shown that the photosynthetic rate of leaves exposed to direct radiation differs from the photosynthetic rate of leaves in shadows (Givnish 1988). To introduce this effect, a "two-leaf" upscaling method has been developed and is referred to in this study as the sun/shade method or SS (Norman 1993; de Pury and Farquhar 1997). The vegetation is partitioned on two big leaves: one leaf for direct, diffuse, and scattered radiation absorption and a second leaf in shadow for the absorption of diffuse and scattered radiation (de Pury and Farquhar 1997; Chen et al. 1999; Mercado et al. 2006). Replacement of the big-leaf with the two-leaf method produced a significant improvement in the weather and climate simulations for all of the scales (Mercado et al. 2006; Sprintsin et al. 2012). The basic assumption of the "two-leaf" approximation is that the canopy can be represented as a block of constant density porous material without a difference between the overstory and the understory vegetation. Multilayer models have been developed to offer more sophisticated information about the canopy structure. Of these models, those that are broadly used are as follows: (a) complex three-dimensional vegetation models with a one-dimensional array (Baldocchi and Harley 1995), (b) two-dimensional arrays (Chen et al. 2008) and (c) three-dimensional arrays (Kobayashi et al. 2012; Good et al. 2013). These models are difficult to introduce into different spatial scale simulations because of their demanding parameterization and computation; however, they produce more accurate simulations of the mass and energy exchange than big-leaf or two-leaf models (Baldocchi et al. 2002).

Ecosystem fluxes result from the complex interaction between the forest canopy (represented by forest micrometeorological conditions and morphological characteristics) and the atmosphere (represented by meteorological conditions on the reference level). Therefore, a physically more realistic parameterization of the distribution of the leaf area density as a function of height, *LAD*(z), and short-wave radiation absorption as the driving force of the most important physical processes representing the air-canopy interaction can reduce errors in the biophysical functionality of the model (Drewry et al. 2010; Chen et al. 2012; Lalic et al. 2013). The level of complexity of the *LAD* parameterization is closely related to the complexity of the vegetation parameterization that can produce the *LAD*-related GPP upscaling method.

The primary goal of this study is to design a new upscaling method based on the improved parameterization of the forest structure and canopy air space micrometeorology to amend the modeling of the forest canopy-atmosphere gas exchange. The basis for the new upscaling method, sun/shade/lad (SSL), is a simple SS approach developed by de Pury and Farquhar (1997). The relationship between the leaf area index (*LAI*) and *LAD*(z) was used to overcome the assumption of a constant *LAI* evenly distributed throughout the forest canopy layers. Therefore, *LAD*(z) introduces an influence on the crown shape, density of the foliage, and partitioning of the contributions of every separate canopy layer to the canopy level GPP. For this purpose, we choose the empirical *LAD*(z) function developed by Lalic and Mihailovic (2004). The primary advantage of this formulation is the realistic representation of the vegetation structural complexity with minimal use of empirical parameters (Lalic et al. 2013). The forest canopy is described only by the following standard nondemanding input vegetation parameters of atmospheric models: forest height, *LAI*, and the height of the maximum *LAD*. The vertical profiles of the sunlit and shaded leaf distribution, photosynthesis parameters, and radiation as a part of the standard SS scaling approach are described as functions of *LAD*(z). The total canopy level GPP was obtained with numerical integration over the depth of the canopy.

To test the primary features of the new upscaling method, both the SS and the SSL methods are applied to the calculated GPP using a SVAT scheme, i.e., the land-air parameterization scheme (LAPS). This scheme was chosen because it is freely available and was tested as the stand-alone version as well as coupled with the Eta numerical weather prediction model in both long-term and short-term simulations (Mihailovic 1996). There is a fair amount of literature explaining the functionality of LAPS (Mihailovic and Kallos 1997; Mihailovic et al. 2000; Mihailovic et al. 2002; Mihailovic et al. 2010). A comparison study was conducted with data collected during the vegetation period on three forest eddy-covariance sites (section 2.1). The sites were chosen to include a high diversity of forest types and structures. LAPS with the photosynthesis rate calculation is presented in section 2.2. Details of the standard SS and proposed SSL upscaling methods are presented in sections 2.3 and 2.4, respectively. The sensitivity of the GPP simulations to the changes in $LAD(z)$ is presented in section 2.5. The comparison study between the SS and SSL upscaling methods and their use in ecosystem modeling is presented in section 3. Section 4 includes our conclusions with a brief elaboration of our future plans of study.

2 Methods

2.1 Datasets

Calibration of the land surface scheme and validation of the proposed upscaling method was performed in the case of three contrasted eddy-covariance (EC) forest sites. The study sites are in the framework of the following two projects: (1) the BOREAS project Northern Study Area Old Black Spruce site (NSA-OBS) and the South Study Area Old Aspen site (SSA-OA) (Sellers et al. 1997b) and (2) the Harvard Forest Environmental Measurement Site (HF-EMS) (Munger and Wofsy 1999), which are presented in Table 1. The datasets used consist of continuous hourly (HF-EMS) and half-hourly (NSA-OBS, SSA-OA) measurements of air temperature, short-wave radiation, humidity, wind speed, precipitation, and CO_2 concentration. These variables were selected because they represent a full set of meteorological input data for LAPS and for the calculation of GPP. Validation of the scheme was performed on EC measurements of latent heat, sensible heat, and CO_2 flux, and the results are presented in section 3.1.

The EC measuring technique provides long-term continuous monitoring of CO_2 transfer in the form of the net ecosystem exchange (NEE). NEE is a balance between the carbon uptake (GPP) and its release through ecosystem autotrophic and heterotrophic respiration, (R_{eco}). To estimate GPP for the model validation, it is necessary to estimate the R_{eco} value. Because the respiration rate is mostly controlled by the temperature and the nighttime CO_2 flux originates only from R_{eco}, the standard procedure for estimating R_{eco} is to use the temperature dependence of the nighttime NEE under daytime conditions. The Lloyd and Taylor (1994) function (Eq. 1) was fitted to the nighttime NEE data to gain the relationship between the ecosystem respiration rate and the temperature, according to the following equation:

$$R_{eco} = R_{ref} \ e^{E_0\left(\frac{1}{T_{ref}-T_0}-\frac{1}{T_{obs}-T_0}\right)}, \qquad (1)$$

where R_{ref} (μmol m^{-2} s^{-1}) represents the base respiration at the reference temperature T_{ref} set to 10 °C, E_0 (°C) is temperature sensitivity, T_{obs} (°C) is the observed temperature, and the parameter T_0 is set to −46.02 °C. During the night, the turbulence is very low, and errors in the measurements of fluxes are common. To overcome this uncertainty, the data used for the nonlinear optimization are the data measured when the friction velocity (u_*) was above 0.25 m s^{-1} (Baldocchi 2003). The GPP from the observation site was calculated as the sum of the measured NEE and the estimated R_{eco} (Yuan et al. 2007).

2.2 Ecosystem modeling

GPP is a measure of the CO_2 exchange between the forest canopy and the atmosphere. This exchange is strongly influenced by plant characteristics and the mass, energy, and momentum transfer between the land surface and the overlying air. In this study, LAPS was used to simulate the land-canopy-atmosphere radiation exchanges, bare soil evaporation, and evapotranspiration (Mihailovic 1996). LAPS includes 12 vegetation types with 16 morphological and physiological plant characteristics and 11 soil textural classes (Mihailovic et al. 2002; Mihailovic 2003). Using seven prognostic equations, this scheme calculates three temperature variables (foliage, soil surface, and deep soil), one interception storage variable, and three soil moisture storage variables. The atmospheric boundary conditions at the reference level include the air temperature, water vapor pressure, wind speed, short-wave and long-wave radiation, precipitation, and CO_2 concentration.

Table 1 Characteristics of the forest EC measurement sites

Dataset	NSA-OBS	SSA-OA	HF-EMS
Latitude	55.88° N	53.63° N	42.54° N
Longitude	98.48° W	106.20° W	72. 17° W
Data (month/year)	06/1996	08/1996	07/2006
Forest type	Evergreen coniferous	Deciduous broadleaf	Deciduous broadleaf
Average canopy height (m)	10	21.5	24
Average *LAI* in vegetation period (m^2 m^{-2})	1.9	2.7	4
Mean temperature (°C)	−3.9	0.4	8.1
Annual precipitation (mm)	590	467	1,100
References	Gower et al. 1997; Kimball et al. 1997; Misson et al. 2007		Munger and Wofsy 1999; Urbanski et al. 2007; Hadley et al. 2009

Energy fluxes are calculated following the resistance representation. The net radiation absorbed by the canopy and the soil is assumed to be partitioned into sensible heat, latent heat, and storage terms, as expressed in the following equations:

$$R_{nf} = \lambda E_f + H_f + C_f \partial T_f / \partial t, \tag{2}$$

$$R_{ng} = \lambda E_g + H_g + C_g \partial T_g / \partial t, \tag{3}$$

where the subscripts f and g refer to the foliage and soil, respectively, R_n is the net radiation (W m^{-2}), λ is the latent heat of vaporization (J kg^{-1}), λE is the evapotranspiration flux (W m^{-2}), H is the sensible heat flux (W m^{-2}), C is the heat capacity per unit area (J K^{-1} m^{-2}), and T is the surface temperature (K) (Sellers et al. 1986; Mihailovic 1996). The sensible and latent heat fluxes in Eqs. 2 and 3 are calculated as the sum of the following: (a) fluxes from the leaf level to the canopy air space (Eqs. A.1 and A.2), (b) fluxes from the ground to the canopy air space (Eqs. A.3 and A.4), and (c) fluxes from the canopy air space to the reference level above the vegetation (Eqs. A.5 and A.6), as presented in Appendix A.

Meteorological drivers, which are essential for running the biochemical photosynthesis model, the temperature, and humidity inside the canopy air space (T_a and e_a in Eqs. A.1–A.6) are calculated diagnostically (Sellers et al. 1986; Mihailovic 1996). The numerical procedure for calculating the leaf temperature (T_f) and the ground surface temperature (T_{gs}) (Eqs. A.1–A.6) based on an implicit backward method is presented in Mihailovic and Eitzinger (2007).

The leaf level photosynthesis rate of the canopy is calculated using a standard mechanistic model developed by Farquhar et al. (1980) and later expanded by von Caemmerer and Farquhar (1981) and Collatz et al. (1991, 1992). The rate of CO_2 assimilation is the sum of the net photosynthesis (A_n) and the leaf dark respiration (R_d) (Eq. 4). The net photosynthesis is defined as the minimum of the Rubisco-limited rate of ribulose bisphosphate (RuBP) carboxylation, A_c (Eq. 6), and the electron transport-limited rate of RuBP regeneration, A_j (Eq. 7), according to the following equations:

$$A = A_n - R_d, \tag{4}$$

$$A_n = \min\left(A_c, A_j\right), \tag{5}$$

$$A_c = V_m \frac{C_i - \Gamma^*}{C_i + K_c(1 + P_o/K_o)}, \tag{6}$$

$$A_j = J \frac{C_i - \Gamma^*}{4\left(C_i + 2\Gamma^*\right)}, \tag{7}$$

where C_i is the internal CO_2 concentration (Pa), K_c=30× 2.1^{Q10} and K_o=30,000× 1.2^{Q10} are the Michaelis-Menten constants (Pa) for CO_2 and oxygen (O_2), respectively, Q_{10}= 0.1(T_c−298.16) is the functional dependency of the leaf temperature T_c, $\Gamma^*=0.105\times K_c P_o K_o^{-1}$ is the CO_2 compensation point (Pa), P_o is the partial pressure of O_2 in air, J is the electron transport rate of the leaf area (μmol CO_2 m^{-2} s^{-1}), V_m is the photosynthetic Rubisco capacity per unit of leaf area (μmol CO_2 m^{-2} s^{-1}), and R_d=0.0089 V_m is the daytime leaf dark respiration rate. The values of the biochemical parameters (V_m, J) have been calculated based on the vertical profiles of the leaf nitrogen content as explained in detail later in this paper.

GPP is calculated using Farquhar's model for the photosynthesis rate per unit of leaf surface, as given in Eqs. 4–7, and scaled up to the canopy level with one of two upscaling techniques, which are presented later in this paper. The input data for the GPP module are the following: the CO_2 concentration and incoming radiation and micrometeorological elements inside the canopy air space calculated by LAPS (leaf temperature, humidity, stomatal and bulk canopy boundary layer resistance). The stomatal resistance is assumed to be a function of atmospheric factors (solar radiation, temperature, and water vapor pressure deficit) and water stress, as proposed by Jarvis (1976) and described in Mihailovic (1996).

2.3 Description of the simple SS upscaling method

The primary goal of upscaling in the context of the vegetation-atmosphere interaction is to provide a reliable procedure to calculate the variable of interest on the canopy level using data obtained on the leaf level. In the simple SS upscaling method, vegetation is considered as a homogenous layer of sunlit and shaded leaves evenly distributed with height. This assumption allows the integration of functions of photosynthetic parameters and equations of radiation absorption over the entire canopy layer with respect to the cumulated *LAI*. However, the forest canopy structure is far more complex than a single homogenous layer. Hence, the SS approach cannot consider, for example, the vertical distribution of leaves, thereby differentiating between deciduous and coniferous trees. To test the primary features of the SS upscaling method, Farquhar's model, presented in section 2.2, is used to calculate the leaf level photosynthesis with respect to the sunlit and shaded leaf fractions (f_{sun} and f_{sha}, respectively), according to the following equations:

$$f_{sun} = e^{-k_b LAI}, \tag{8}$$

$$f_{sha} = 1 - f_{sun}, \tag{9}$$

where k_b represents the beam radiation extinction coefficient taken as 0.5/cosθ (θ is the zenith angle).

A vast number of papers have been offered (Ingestad and Lund 1986; Norman 1993; Niu et al. 2005; Kimball et al. 1997) that show that V_m is linear with the leaf nitrogen content. Therefore, the decay of the nitrogen (N) and leaf photosynthetic capacity (V_0) can be expressed similar to that of the irradiance decay with the canopy layer depth, according to the following equation:

$$N = N_0 e^{-k_n LAI}, \tag{10}$$

where N_0 is the concentration of nitrogen at the top of the canopy, and k_n is the leaf nitrogen content decay rate with canopy depth taken as 0.3, in accordance with de Pury and Farquhar (1997).

The leaf photosynthetic capacity V_0 is a function of the ratio of the photosynthetic capacity to the leaf nitrogen χ_n (mmol m^{-2} s^{-1}), according to the following equation:

$$V_0 = \chi_n N. \tag{11}$$

With respect to Eqs. 8–9 and the sun and shaded fractions of the leaf area, we can write Eq. 11 in the form of the following equation:

$$V_{m,\mathrm{sun}} = \int_0^{L_c} V_0(L) f_{\mathrm{sun}}(L) dL = L_c \chi_n N_0 \left[\frac{1 - e^{(-k_n - k_b L_c)}}{k_n + k_b L_c} \right]. \tag{12}$$

Integration is performed with respect to the cumulative LAI (L_c), which is taken as a description of the canopy depth. Analogous to Eqs. 8–9, we can express the following:

$$V_{m,sha} = 1 - V_{m,\mathrm{sun}}, \tag{13}$$

where $V_{m,\mathrm{sun}}$ and $V_{m,\mathrm{sha}}$ represent the photosynthetic Rubisco capacity of the sunlit and shaded fractions of the leaf area, respectively (μmol CO_2 m^{-2} s^{-1}).

The electron transport rate of the sunlit and shaded fractions of the leaf area (μmol CO_2 m^{-2} s^{-1}) is also a function of the vertical nitrogen gradient, according to the following equation:

$$J_{m,sun/sha} = 29.1 + 1.6 V_{m,sun/sha}. \tag{14}$$

The radiation absorbed by the sun and shaded leaf fractions and integrated over the entire canopy is described in detail in de Pury and Farquhar (1997).

Finally, photosynthesis of both fractions is calculated with the corresponding parameters, according to the following equation:

$$A_{SS/sum,sun} = \left[\min\left(A_{c,sun}, A_{j,sun}\right) - R_{d,sun}\right] + \left[\min\left(A_{c,sha}, A_{j,sha}\right) - R_{d,sha}\right]. \tag{15}$$

2.4 Description of the SSL upscaling method

The SSL upscaling method is based on the combination of the SS upscaling method with a multilayer approach that considers the canopy structure. As a result, we can obtain the positive effects of both methods, which are the efficiency of the SS method and the physical accuracy of the multilayer canopy model. Application of the multilayer approach in the GPP calculation requires very detailed knowledge about the vegetation structure, the parameterization of photosynthesis and the vertical distribution of the photosynthetic active radiation (PAR) (Kotchenova et al. 2004). The CO_2 and air temperature can be considered constant within the whole canopy layer (Calvet et al. 1998).

The forest canopy structure in environmental models is often described using the amount of leaves and stems, and their spatial distribution is represented by LAI and LAD, respectively. The relationship between LAI and LAD can be expressed in the following way:

$$LAI = \int_0^h LAD(z) dz. \tag{16}$$

This formulation provides layers of integration as separate canopy layers, and $LAD(z)$ provides a structural parameter that can express the vertical heterogeneity of the forest canopy.

The leaf area density profile is typically obtained from field observations (Kotchenova et al. 2004; Treuhaft et al. 2002). This procedure made its use in SVAT schemes of different scales difficult. To avoid this problem, we used an empirical relation for $LAD(z)$, proposed by Lalic and Mihailovic (2004), in the form of the following equation:

$$LAD(z) = L_m \left(\frac{h - z_m}{h - z} \right)^n e^{n(1 - (h - z_m)/(h - z))}, \tag{17}$$

where $n = \begin{cases} 6 & 0 \le z < z_n \\ \frac{1}{2} & z_m \le z \le h \end{cases}$.

The suggested relationship is based on the following primary forest canopy structural characteristics: tree height h, maximum value of LAD L_m, and the corresponding height z_m (Mix et al. 1994; Law et al. 2001; Lalic and Mihailovic 2004) presented in Fig. 1. This formula can be applied over a broad range of forest canopies. The classification is based on the ratio between the z_m and h parameters as follows: (a) z_m/h=0.2 for oak and silver birch, (b) 0.2<z_m/h<0.4 for common maple, and (c) z_m/h=0.4 for pine (Kolic 1978).

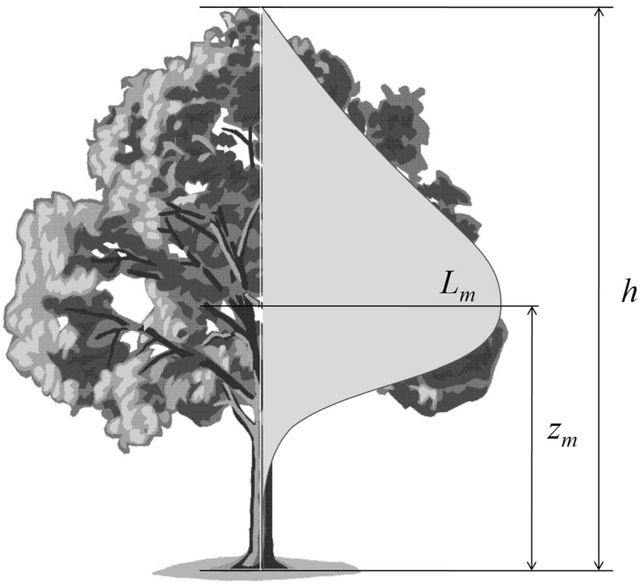

Fig. 1 Graphical presentation of $LAD(z)$ with corresponding values used in Eqs. 16 and 17

The combination of the standard Lambert-Beer's law describing radiation penetration through tall vegetation $I(z)=I_0\exp(-kLAI)$ and the leaf area density described in Eq. 15 provides a new radiation profile according to the following equation:

$$I(z)=I_0 e^{-k\int_h^z LAD(z)dz}, \tag{18}$$

where $I(z)$ represents the PAR that reaches height z inside the canopy air space, and $k=k'/\cos\theta$ where k' is the extinction coefficient depending on the forest type, and θ is the zenith angle. A physically realistic radiation profile provides information about the forest canopy structure that can be used in further calculations (Bodin and Franklin 2012). The radiation profile from Eq. 18 was tested against 615 profiles of the PAR observed between 0800 and 1800 local mean time for 72 days at two locations in the Amazon forest, and the results are presented in Lalic et al. 2013.

In the SS upscaling method, the relationships representing the vertical fractions of the sunlit leaves and shaded leaves (Eqs. 8 and 9) are written as the exponential part of the Lambert-Beer's law; therefore, they can be expressed as a function of $LAD(z)$ according to the following equations:

$$f_{\text{sun}}(z)=e^{-k\int_h^z LAD(z)dz}, \tag{19}$$

$$f_{\text{sha}}(z)=1-f_{\text{sun}}(z). \tag{20}$$

If we know the relationships for the fractions of the sunlit and shaded leaves, we can easily determine the sunlit and shaded leaf area indices as a function of $LAD(z)$ according to the following equations:

$$LAI_{\text{sun}}=\int_0^{Lc} f_{\text{sun}}(L)dL=\int_0^{Lc} e^{-k\int_h^z LAD(z)dz} dL, \tag{21}$$

and

$$LAI_{\text{sha}}=LAI-LAI_{\text{sun}}. \tag{22}$$

The radiation profiles of the sunlit (I_{sun}) and shaded (I_{sha}) leaf irradiance values used in the SS model developed by de Pury and Farquhar (1997), which are based on the multilayer radiation model, are expressed in this study according to the following equations:

$$I_{\text{sun}}=\int_0^{Lc} I_{\text{beam}} e^{-k_b\int_h^z LAD(z)\,dz} dL+\int_0^{Lc} I_{\text{diff}} e^{-k_d\int_h^z LAD(z)\,dz} dL$$
$$+\int_0^{Lc} I_{\text{sca}} e^{-k_s\int_h^z LAD(z)\,dz} dL, \tag{23}$$

and

$$I_{\text{sha}}=\int_0^{Lc} I_{\text{diff}} e^{-k_d\int_h^z LAD(z)\,dz} dL+\int_0^{Lc} I_{\text{sca}} e^{-k_s\int_h^z LAD(z)\,dz} dL, \tag{24}$$

where I_{beam}, I_{diff}, and I_{sca} are the radiation profiles of beam, diffuse, and scattered radiation, respectively. The radiation profiles are calculated using Eq. 19, with parameter k associated with a certain type of radiation according to de Pury and Farquhar (1997).

The set of equations present in the SS scaling method representing the vertical profiles of the photosynthetic parameters are defined with the relationship in the form of Eq. 15. The leaf nitrogen profile, $N(z)$, can be written according to the following equation:

$$N(z)=N_0 e^{-k_n LAI}=N_0 e^{-k_n\int_h^z LAD(z)dz}. \tag{25}$$

Using the relationship between $N(z)$ and V_m present in the SS method, the following expression can be written:

$$V_m(z) = \chi_n N(z). \tag{26}$$

where $V_{m,\mathrm{sun}}$ and $V_{m,\mathrm{sha}}$ are functions of the crown shape defined by $LAD(z)$ according to the following equations:

$$V_{m,\mathrm{sun}} = \int_0^{Lc} V_m(L) f_{\mathrm{sun}}(L) dL = \int_0^{Lc} \chi_n N_0 e^{-k_n \int_h^z LAD(z)\,dz} e^{-k \int_h^z LAD(z)\,dz} dL, \tag{27}$$

$$V_{m,\mathrm{sha}} = 1 - V_{m,\mathrm{sun}}. \tag{28}$$

The SSL upscaling method is based on the use of profiles of the sun and shade fractions of irradiance (I_{sun} and I_{sha}, respectively), the profile of nitrogen ($N(z)$), and the photosynthetic capacity ($V_{m,\mathrm{sun}}$ and $V_{m,\mathrm{sha}}$) in numerical integrations to calculate the assimilation of the leaf surface in the volume having a height of h_i. The contribution of every integration layer, incorporating the tree crown shape into the upscaling process, can be written according to the following equation:

$$A_{\mathrm{SSL}/\mathrm{sum,sun}} = \sum_{i=1}^{N} \left\{ \left[\min\left(A_{c,\mathrm{sun}}, A_{j,\mathrm{sun}}\right) - R_{d,\mathrm{sun}}\right] + \left[\min\left(A_{c,\mathrm{sha}}, A_{j,\mathrm{sha}}\right) - R_{d,\mathrm{sha}}\right] \right\}_{\mathrm{layer}}(h_i). \tag{29}$$

2.5 Sensitivity tests

2.5.1 The impact of the forest canopy structure on the GPP

To examine the impact of the forest canopy structure on the GPP upscaled by the SSL scaling method, a sensitivity test with different $LAD(z)$ values was performed; the GPP is calculated using a set of meteorological data specific for midday without clouds on the HF-EMS site. Photosynthetically active radiation is set to be 1,500 μmol m^{-2} s^{-1}, the temperature is set to 20 °C, the partial pressure of CO_2 in the canopy air space is set to 38 Pa, the relative humidity is set to 65 %, the atmospheric pressure is set to 10^5 Pa, and the LAI is set to 3.5 m^2/m^2. To include different vertical structures of the forest canopy, parameter z_m is changed from 0.1 h to 0.9 h in steps of 0.1 in which h is the forest height set to 25 m. Figure 2 shows the GPP values calculated using the SSL upscaling technique for different sun and shaded irradiance profiles (the sun fraction is on the left panel) and LAD profiles (right panel). This figure shows that changes in $LAD(z)$ (varying z_m from 0.1 h to 0.9 h) result in GPP changes by 7 μmol m^{-2} s^{-1}, indicating that small changes in the canopy structure can produce noticeable changes in the upscaled GPP using the SSL method.

Therefore, it is accurate to assume that when used in environmental and land-atmosphere gas exchange models, the SSL upscaling method can make a difference in the case of long-term simulations by avoiding systematic errors, such as the overestimation or underestimation of the GPP. For short-term simulations, changes in forest foliage density, presented with different vertical profiles of $LAD(z)$, can represent different forest management practices, such as the thinning of the forest. This procedure can change the amount of irradiance penetrating the forest canopy layer and result in an increasing GPP. From a modeler's viewpoint, the consequent changes can be easily performed by changing the parameter z_m.

2.5.2 Impact of the forest canopy structure on GPP partitioning

The vertical distribution of LAI described with the $LAD(z)$ function provides the opportunity to simulate the canopy vertical heterogeneity in terms of different species dominating the upper and lower parts of the forest. The SSL upscaling method was tested for its capability to partition the GPP on the upper and lower forest floor. A sensitivity test was performed according to settings from the 2.5.1 sensitivity tests. For the upperstory (LAI_{upper}) and understory (LAI_{under}), we used different values of LAI set at 2 and 3, respectively. We assumed a constant temperature and CO_2 concentration inside the canopy air space.

Figure 3 depicts the impact of upperstory and lowerstory partitioning on the calculated GPP. A uniformly distributed leaf area produces a larger GPP in both the upper and lower stories, whereas flux partitioning related to the canopy architecture provides a positive answer to

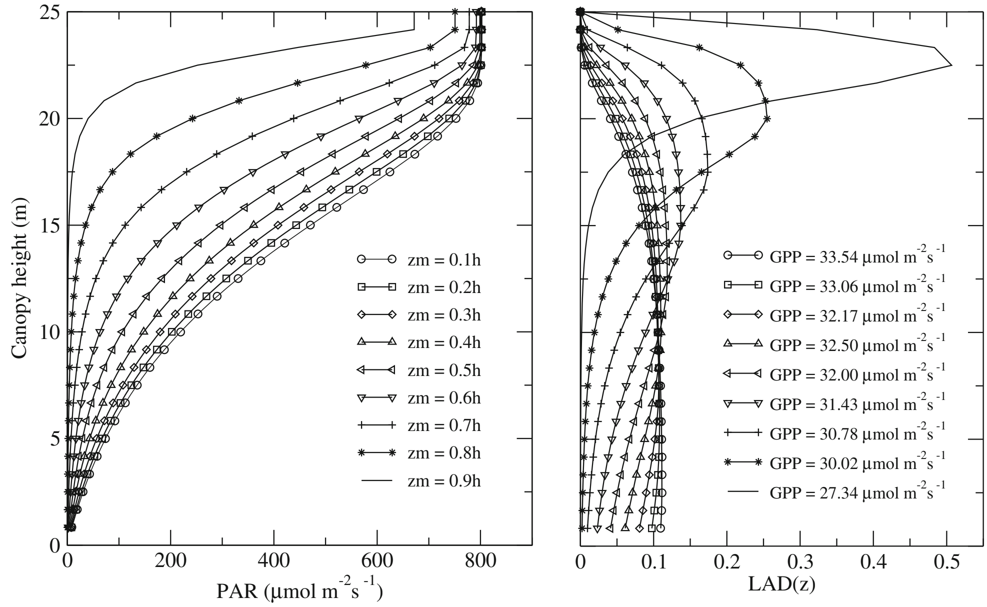

Fig. 2 Beam PAR vertical profiles (*left panel*) with the corresponding *LAD*(*z*) profiles and the calculated GPP (*right panel*) for the different z_m values

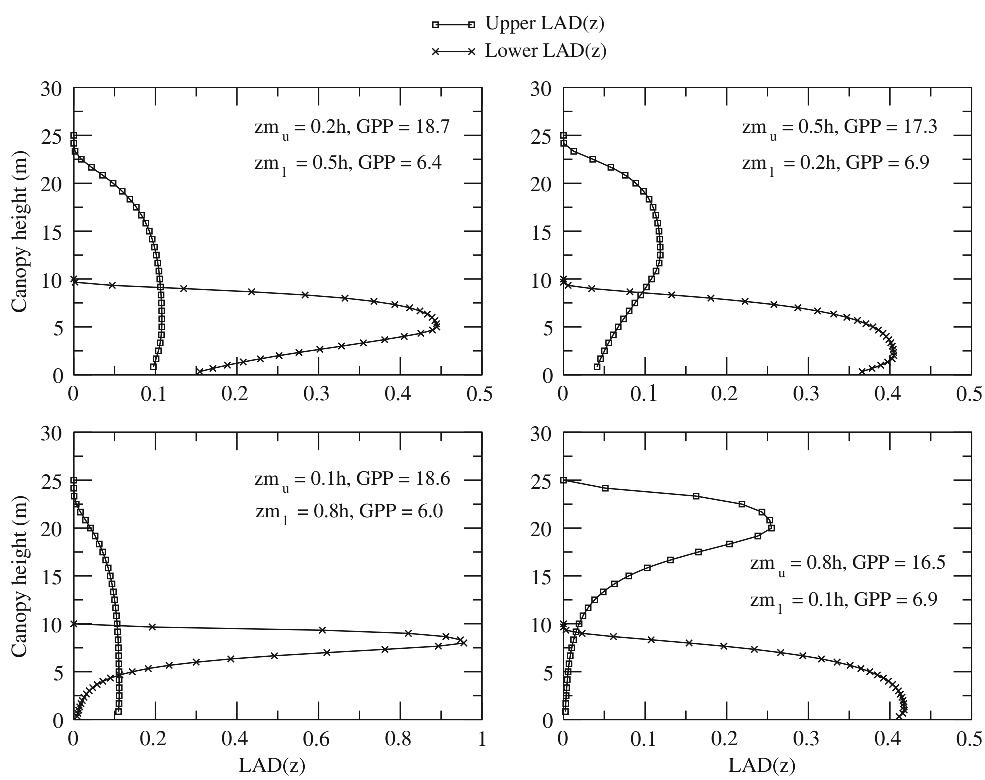

Fig. 3 *LAD*(*z*) profiles for the upperstory and understory vegetation with the corresponding GPP (μmol m^{-2} s^{-1})

the question: "Is there optimal canopy architecture for the maximization of the CO_2 uptake?" (Song et al. 2012). The SSL upscaling method demonstrated that the optimal architecture is characterized by a uniform distribution of canopy leaves. Figure 3 shows that a denser vegetation in the overstory does not have a significant influence on the understory GPP, which can be up to 40 % of the total GPP; this result has also been observed by Misson et al. (2007).

3 Results and discussion

3.1 Validation of the LAPS and GPP simulations

To investigate the performance of LAPS in calculating meteorological drivers for GPP simulations, the scheme was coupled with the basic Farquhar's GPP module scaled up with the SS approach. The coupled model was validated using 1 month of hourly data collected during the vegetation period from the HF-EMS site (Table 1). An important feature of the HF-EMS site is the uniform distribution of the homogenous forest canopy, making it ideal for the application of the SS scaling method. This location is chosen to avoid errors in simulations caused because of the vertical heterogeneity of vegetation.

The computed values of the temperature, relative humidity, sensible heat flux, latent heat flux, and GPP are plotted against the observed values from the EC tower (Fig. 4). The comparison showed a small dispersion and a large correlation coefficient for all of the presented values. However, a slight deviation can be identified in the calculation of the latent heat flux, λE (Fig. 4d), in which the calculated values are systematically higher than the observed values. Micrometeorological variables calculated using LAPS along with the concentration of CO_2 and PAR were used for the calculation of GPP, as presented in sections 2.2, 2.3, and 2.4 (Fig. 4e). The vegetation parameters used in the simulations can be found in Table 2. The GPP comparison study (Fig. 4e) demonstrates a high performance of the SS upscaling method and justifies the rationale for using the SS approach as a theoretical basis for the development of the SSL upscaling method.

3.2 Comparison of the SS and SSL upscaling methods

The impact of the proposed SSL method for upscaling the leaf level photosynthesis rate to the forest level was tested against the standard SS approach on three forest EC sites, as presented in section 2.1. The site characteristics are given in Table 1; the morphological and biophysical characteristics used in the calculations are given in Table 2. To quantify the validity of the GPP calculation and the impact of the upscaling method on the calculated GPP values, we performed an error analysis based on the methodology employed by Pielke (1984) and Mahfouf (1990). This error analysis employs the calculation of the root-mean squared error (RMSE, ν) of the daily values of the GPP for the SS (ν_{SS}) and SSL (ν_{SSL}) upscaling methods along with the standard deviations (SD, σ) of the observed (σ_o) and simulated data ($\sigma_{SS,}$ σ_{SSL}). According to the abovementioned authors, the simulation is performed more realistically if the following conditions are met: (a) ν is less than σ_o and (b) σ is close to σ_o. The results of the comparison between the calculated GPP scaled up with the SS and SSL methods, and the observed values along with the error analysis of the daily values for the three sites are presented in Figs 5, 6, and 7.

From the HF-EMS site, we used a continuous set of data from the 152 to the 181 days of year (DOY) (Munger and Wofsy 1999). The results presented in Fig. 5 show small differences in the GPP upscaled value using the SS and SSL methods. This result is primarily because the homogenous vegetation layer is dominated by red oak (*Quercus rubra*). The parameter z_m, which defines the forest structure in the $LAD(z)$ profile, is set to 0.7 h for this site. In this case, the impact of the canopy structure on the GPP calculation is unclear. Differences can be identified when the radiation inside the vegetation layer is overestimated using the SS approach, causing an overestimation in the GPP calculation. The reason for the overestimation of the Beer's law-based irradiance profiles has been described in detail by Lalic et al. 2013. Additionally, special attention should be devoted to the small values of the GPP measured at the end of the period of interest (the last 7 days). During these days, we can observe that both approaches failed to accurately reproduce the GPP values. The error analysis performed for this site shows the following: (a) ν_{SSL} was greater than ν_{SS} for only 3 days, (b) σ_{SSL} was closer to σ_o than σ_{SS} in 50 % of the cases, and (c) ν_{SSL} was greater than σ_o in only three cases. The range of errors, the maximal values of RMSE and SD, and the corresponding DOY are given in Table 3.

We used a continuous set of data collected from the 196 to 218 DOY to exclude the days without data from the NSA-OBS site (Newcomer et al. 2000). The difficulty in using the SS approach at this site originates from the nonhomogeneous vertical structure of the

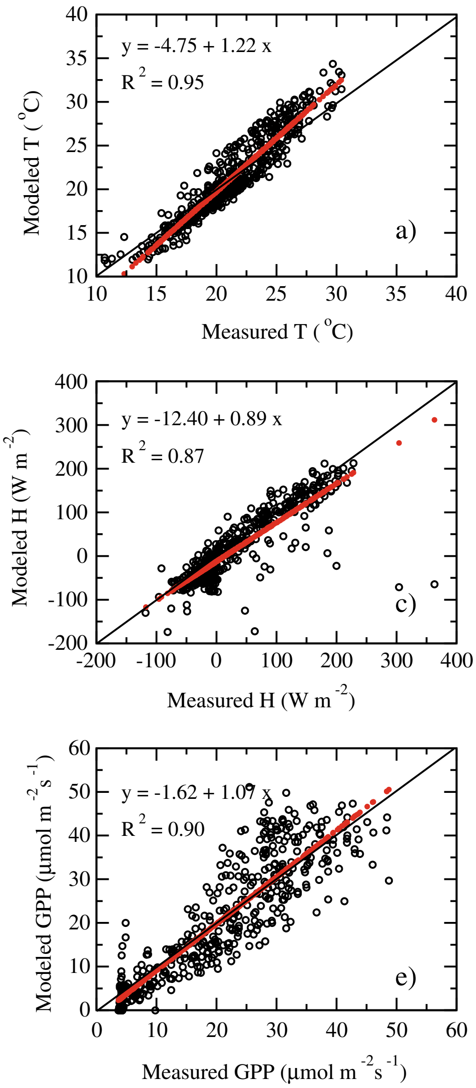

Fig. 4 The measured and modeled values of **a** temperature T, **b** relative humidity R_h, **c** sensible heat flux H, **d** latent heat flux λE, and **e** GPP for the HF-EMS site

evergreen conifers forest dominated with old black spruce (*Picea mariana*). Parameter z_m, which describes the forest structure in the $LAD(z)$ profile, is set to 0.8 h for this site. The high density of the vegetation and the emphasized vertical canopy structure has a significant impact on the results obtained using the SSL upscaling method. The results of the error analysis presented in Fig. 6 show the following: (a) ν_{SSL} was greater than ν_{SS} for only 7 days, (b) σ_{SSL} was closer to σ_o than σ_{SS} in 70 % of the cases, and (c) ν_{SSL} was greater than σ_o for only four cases. We also noted that the use of the SS method produces overestimated values of the GPP, which can be explained by the omitted impact of the forest structure on the GPP calculation. This impact is less evident in cases in which there is a sudden shift in the measured values (i.e., days 205 and 216) when the error of the SS approach is smaller because of overestimation. In the case of the NSA-OBS site, the range of errors, the maximal values of RMSE and SD, and the corresponding DOY are given in Table 3.

From the SSA-OA site, we used a continuous set of data collected from the 213 to 243 DOY (Newcomer et al. 2000). This site is characterized by strong understory vegetation. The overstory is predominantly aspen (*Populus tremuloides* Michx), whereas the understory is primarily composed of hazelnut (*Corylus cornuta* Marsh) that is approximately 2 m tall. Parameter z_m for this forest is set to 0.85 h because of the dense

Table 2 The values of the biochemical, morphological, and aerodynamic characteristics used in the numerical experiments for the two land cover types in this study

Parameters	Broadleaf deciduous	Evergreen conifers	References
Biochemical parameters			
Maximal carboxylation capacity, V_{cmax} (mol m^{-2} s^{-1} at 25 °C)	57.7±21.2	62.5±24.7	Wullschleger 1993; Medlyn et al. 1999; Niu et al. 2005; Kattge et al. 2009
Leaf nitrogen content, N_0 (g m^{-2})	1.74+0.71	3.10+1.35	Kattge et al. 2009
Ratio of photosynthetic capacity to leaf nitrogen, χ_n (m^2 g^{-1})	0.59	0.33	
Morphological and aerodynamic characteristics			
Canopy bottom height, h_b (m)	6	5	LAPS vegetation parameters
Foliage emissivity ε_f	0.95	0.97	Campbell and Norman 1998
Displacement height, d (m)	0.8	0.6	LAPS vegetation parameters
Fractional cover, σ_{fc}	0.8	0.9	LAPS vegetation parameters
Effective roughness length, z_g (m)	0.005	0.005	LAPS vegetation parameters
Roughness length, z_0 (m)	0.8	1.1	Campbell and Norman 1998

understory, which does not allow the radiation to penetrate to the soil surface. In this case, the forest architecture strongly influences the surface fluxes and the GPP. The results of the error analysis are presented in Fig. 7. Compared with the HF-EMS and NSA-OBS sites, the results obtained are strongly influenced by the canopy architecture and layers. Figure 7 shows the following: (a) for seven out of 30 days, the ν_{SSL} was greater than the ν_{SS}, (b) σ_{SSL} was closer to σ_o than σ_{SS} in 75 % of the cases, and (c) ν_{SSL} was greater than σ_o for only 1 day (Table 3).

The calculations for the SSA-OA site demonstrated the SSL scaling efficiency in calculating the GPP of the highly heterogeneous forest canopy with different layers. From a structural viewpoint, the GPP at the SSA-OA site can be represented as the sum of the GPP gained with the upper vegetation and the contribution of the lower vegetation. The problem of canopy flux partitioning is easily solved with the SSL type of upscaling, as presented in section 2.5, which explains why the SS upscaling method produces an overestimation of the GPP on all three sites.

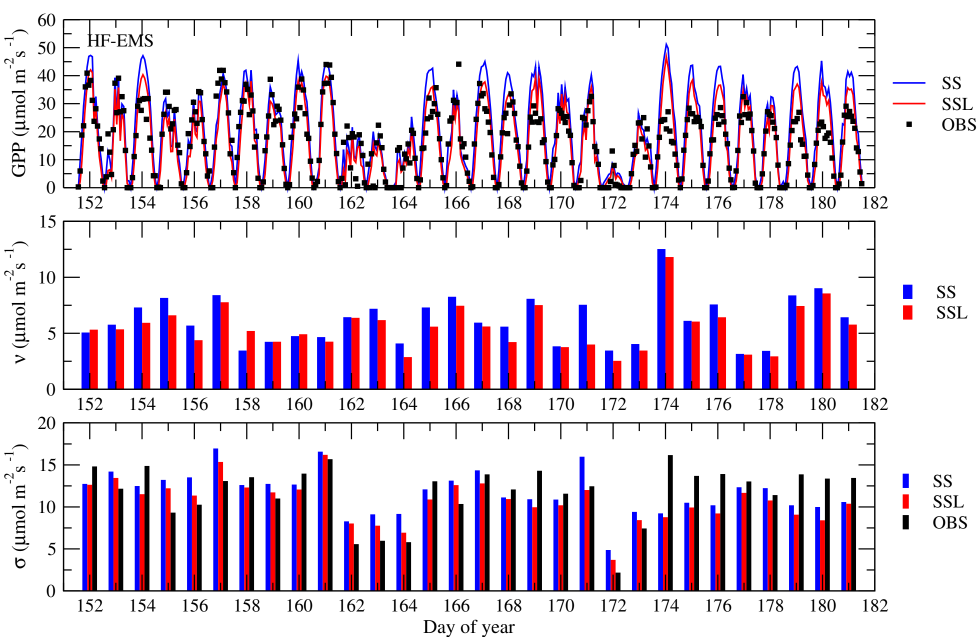

Fig. 5 The GPP (μmol m^{-2} s^{-1}) observed (*OBS*) and upscaled using the SS and SSL methods (*first plot*), followed by the error analysis with RMSE (ν_{SS} and ν_{SSL}) (*second plot*) and the standard deviation of the simulated (σ_{SS}, σ_{SSL}) and observed (σ_o) data (*third plot*) for the HF-EMS site

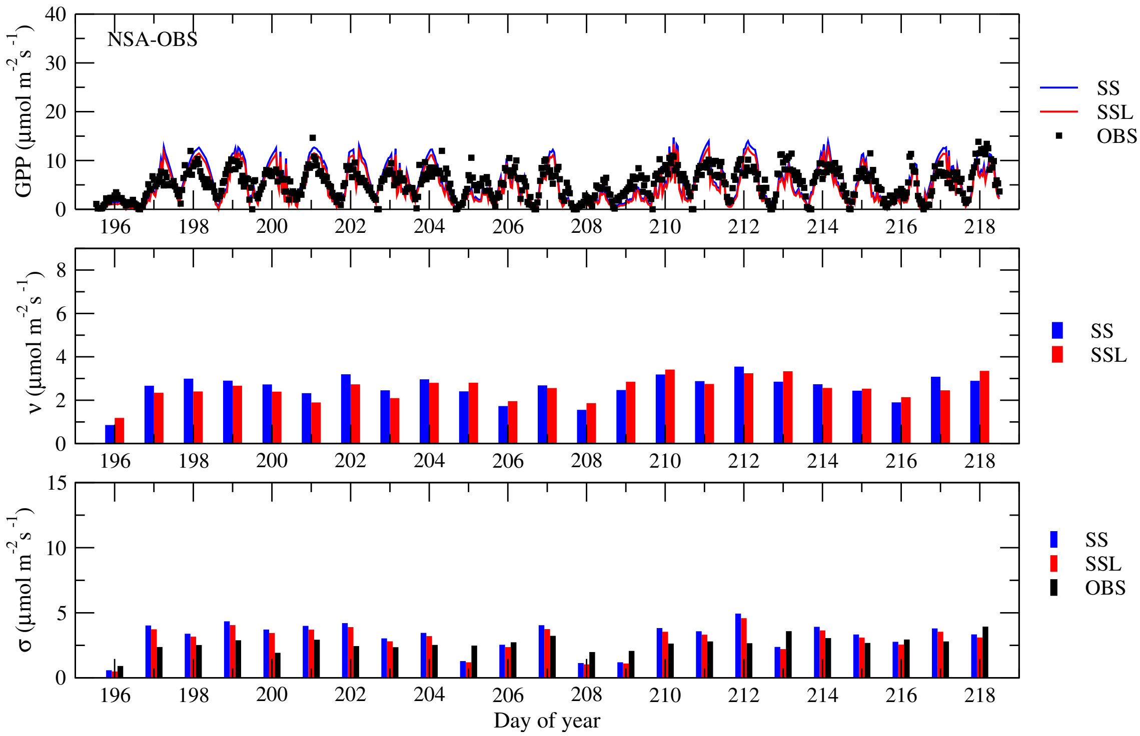

Fig. 6 The GPP (μmol m^{-2} s^{-1}) observed (*OBS*) and upscaled using the SS and SSL methods (*first plot*), followed by the error analysis with RMSE (ν_{SS} and ν_{SSL}) (*second plot*) and the standard deviation of the simulated (σ_{SS}, σ_{SSL}) and observed (σ_o) data (*third plot*) for the NSA-OBS site

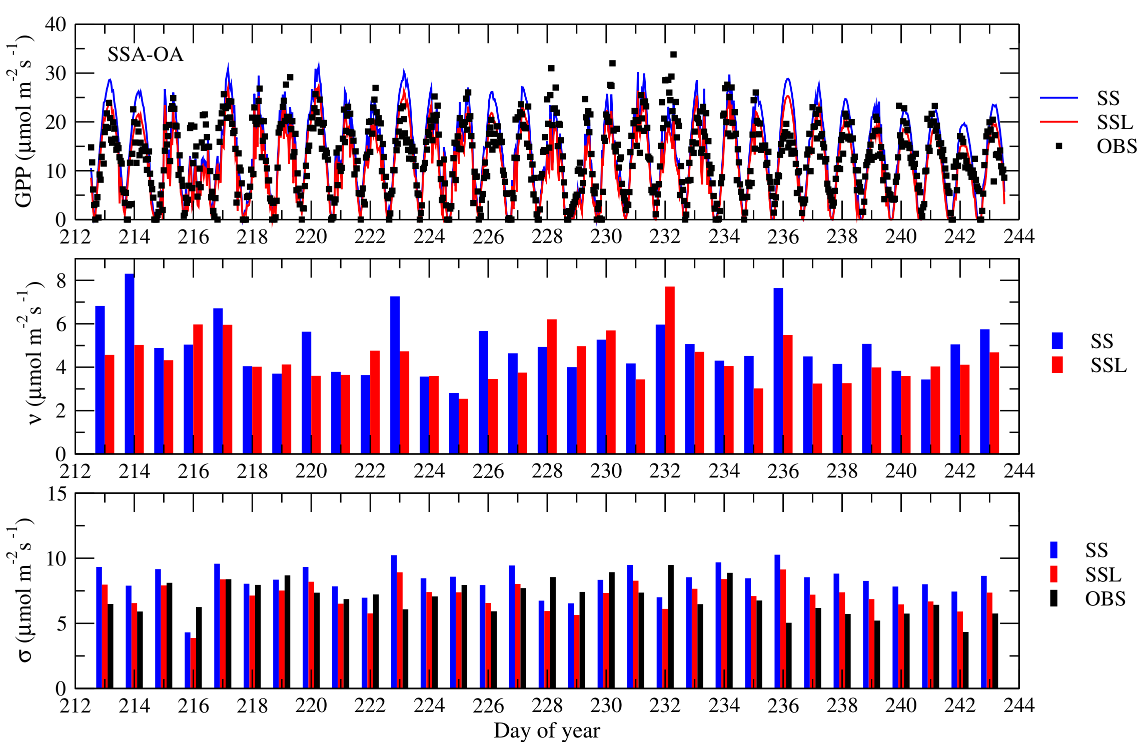

Fig. 7 The GPP (μmol m^{-2} s^{-1}) observed (*OBS*) and upscaled using the SS and SSL methods (*first plot*), followed by the error analysis with RMSE (ν_{SS} and ν_{SSL}) (*second plot*) and the standard deviation of the simulated (σ_{SS}, σ_{SSL}) and observed (σ_o) data (*third plot*) for the SSA-OA site

Table 3 Statistical parameters (RMSE in μmol m^{-2} s^{-1}, SD in μmol m^{-2} s^{-1}), their range, and the corresponding DOY

Statistical parameters	HF-EMS		NSA-OBS		SSA-OA	
Upscaling method	SS	SSL	SS	SSL	SS	SSL
Range of RMSE	3.1–9.0	4.2–10.0	0.8–3.2	1.2–3.3	2.8–7.6	2.5–6.2
Maximal RMSE	12.5	11.1	3.5	3.4	8.3	7.7
Day of max RMSE	174	174	212	210	214	236
Range of SD	4.8–16.5	3.6–15.4	0.5–4.3	0.4–4.0	4.3–9.6	3.8–8.8
Maximal SD	16.9	16.3	4.9	4.5	10.2	9.0
Day of max SD	157	161	212	212	236	236
Range of SD observed	2.4–16.7		0.9–3.5		4.6–9.4	
Maximal SD observed	16.8		3.9		9.5	
Day of max SD observed	161		218		215	

4 Conclusions and discussions

The primary goal of this study was to improve the actual SS upscaling method for the GPP calculation on the canopy level by introducing vertical heterogeneity of the forest canopy and the appropriate vertical profile of solar radiation. We considered and discussed the profiles of the solar radiation and leaf area density distribution and their impact on the parameterization of the CO_2 exchange between the forest canopy and the atmosphere in coupled land-atmosphere schemes for environmental modeling. Improvement of the actual SS upscaling method is achieved by the introduction of vertical heterogeneity of the forest canopy and the appropriate vertical profile of the solar radiation. This goal was implemented through the following steps:

1. The existing SVAT scheme, LAPS, was coupled with Farquhar's biophysical model to calculate the leaf level photosynthesis rate;
2. The canopy GPP was calculated using the SS and SSL upscaling methods. The SSL method is designed based on the SS method and is upgraded by the introduction of the more realistic physical profiles of PAR(z) and $LAD(z)$ to account for the vertical heterogeneity of the forest canopy structure;
3. The calculated GPP is compared with observations to test the introduced assumptions.

The obtained results indicate the following:

1. For all of the sites, the SSL approach produced smaller errors in the GPP calculation with smaller maximal errors.
2. The standard deviation of the data gain with the SSL approach was closer to the standard deviation of the observed data for all of the sites.

These results imply that the suggested SSL upscaling method is quite realistic in simulating GPP and the canopy structure impact on the simulated GPP. The simplicity behind the SSL method enables its general use, particularly because it includes the standard SS approach to parameterization. These characteristics of the SSL approach make it suitable for long-term climatic simulations or short-term ecological or forest management simulations. This approach also provides insight into the influence of the different canopy structures, flooring, densities, and disturbance to the total ecosystem GPP simulations.

Acknowledgments The research work described in this paper was realized as a part of the project "Studying climate change and its influence on the environment: impacts, adaptation, and mitigation" (43007) financed by the Ministry of Education and Science of the Republic of Serbia within the framework of integrated and interdisciplinary research for the period 2011–2014.

Appendix A

Flux partitioning in LAPS

1. Fluxes from the leaf level to the canopy air space are represented in the following equations:

$$H_c = \rho c_p \frac{2(T_c - T_a)}{r_b}, \tag{A.1}$$

$$\lambda E_c = (e_*(T_c) - e_a)\frac{\rho c_p}{\gamma}\left(\frac{W_c}{r_b} + \frac{1 - W_c}{r_b + r_c}\right), \tag{A.2}$$

where c refers to the canopy, and the other values are ρ, air density (kg m^{-3}); C_p, specific heat of the air at constant pressure (J kg^{-1} K^{-1}); γ, the psychrometric constant (hPa K^{-1}); T_c, leaf temperature (K); T_a, temperature of the canopy air space (K); r_b bulk canopy boundary layer resistance (s m^{-1}); and r_c is the bulk canopy stomatal resistance (s m^{-1}); $e_*(T_c)$ saturated vapor pressure for the canopy temperature (hPa); e_a, vapor pressure inside the canopy air space (hPa); W_c, part of the vegetation wet surface; and λ is the latent heat of evaporation.

2. Fluxes from the ground to the canopy air space are represented in the following equations:

$$H_{gs} = \rho c_p \frac{2(T_{gs} - T_a)}{r_d}, \quad (A.3)$$

$$\lambda E_{gs} = \frac{(\alpha_s e_*(T_{gs}) - e_a)}{r_b + r_d} \frac{\rho c_p}{\gamma}, \quad (A.4)$$

where gs refers to the ground surface; the other values are T_{gs}, ground surface temperature; $e_*(T_{gs})$, saturated vapor pressure for the ground surface temperature; r_d is the aerodynamic resistance between the soil surface and the canopy air space (s m^{-1}); and α_s is the soil wetness factor (Mihailovic et al. 1995).

3. Fluxes from the canopy air space to the reference level above vegetation are represented in the following equations:

$$H_r = H_c + H_{gs} = \rho c_p \frac{(T_a - T_r)}{r_a}, \quad (A.5)$$

$$\lambda E_r = \lambda E_c + \lambda E_{gs} = \frac{\rho c_p}{\gamma} \frac{(e_a - e_r)}{r_a}, \quad (A.6)$$

where r is the reference level; the other values are T_r, air temperature at the reference level; e_r, vapor pressure at the reference level above the vegetation; and r_a is the aerodynamic resistance (s m^{-1}).

References

Baldocchi DD (2003) Assessing the eddy covariance technique for evaluating carbon dioxide exchange rates of ecosystems: past, present and future. Glob Change Biol 9:479–492. doi:10.1046/j.1365-2486.2003.00629.x

Baldocchi DD, Harley PC (1995) Scaling carbon dioxide and water vapour exchange from leaf to canopy in a deciduous forest. II. Model testing and application. Plant Cell Environ 18:1157–1173. doi:10.1111/j.1365-3040.1995.tb00626.x

Baldocchi DD, Wilson KB, Gu L (2002) How the environment, canopy structure and canopy physiological functioning influence carbon, water and energy fluxes of a temperate broad-leaved deciduous forest—an assessment with the biophysical model CANOAK. Tree Physiol 22(15–16):1065–1077. doi:10.1093/treephys/22.15-16.1065

Ball J, Woodrow I, Berry J (1987) A model predicting stomatal conductance and its contribution to the control of photosynthesis under different environmental conditions. In: Biggens J (ed) Progress in photosynthesis research, vol IV. Martinus Nijhoff Pub, Dordrecht, pp 221–224

Bodin P, Franklin O (2012) Efficient modeling of sun/shade canopy radiation dynamics explicitly accounting for scattering. Geosci Model Dev 5:535–541. doi:10.5194/gmd-5-535-2012

Calvet J-C, Noilhan J, Roujean J-L, Bessemoulin P, Cabelguenne M, Olioso A, Wigneron J-P (1998) An interactive vegetation SVAT model tested against data from six contrasting sites. Agric For Meteorol 92:73–95. doi:10.1016/S0168-1923(98)00091-4

Campbell GS, Norman JM (1998) An introduction to environmental biophysics, 2nd ed, Springer, p 286

Chen JM, Liu J, Cihlar J, Guolden ML (1999) Daily canopy photosynthesis model through temporal and spatial scaling for remote sensing applications. Ecol Model 124:99–119. doi:10.1016/S0304-3800(99)00156-8

Chen Q, Baldocchi D, Gong P, Dawson T (2008) Modeling radiation and photosynthesis of a heterogeneous savanna woodland landscape with a hierarchy of model complexities. Agric For Meteorol 148(6–7):1005–1020. doi:10.1016/j.agrformet.2008.01.020

Chen JM, Mo G, Pisek J, Deng F, Ishozawa M, Chan D (2012) Effects of foliage clumping on global terrestrial gross primary productivity. Glob Biogeochem Cycles 26, GB1019. doi:10.1029/2010GB003996

Collatz GJ, Ball JT, Grivet C, Berry JA (1991) Physiological and environmental regulation of stomatal conductance, photosynthesis and transpiration: a model that includes a laminar boundary layer. Agric For Meteorol 54:107–136. doi:10.1016/0168-1923(91)90002-8

Collatz J, Ribas-Carbo M, Berry J (1992) Coupled photosynthesis-stomatal conductance model for leaves of C4 plants. Aust J Plant Physiol 19:519–538. doi:10.1071/PP9920519

de Pury DGG, Farquhar GD (1997) Simple scaling of photosynthesis from leaves to canopies without the errors of big-leaf models. Plant Cell Environ 20(5):537–557. doi:10.1111/j.1365-3040.1997.00094.x

Drewry DT, Kumar P, Long S, Bernacchi C, Liang X-Z, Sivapalan M (2010) Ecohydrological responses of dense canopies to environmental variability: 1. Interplay between vertical structure and photosynthetic pathway. J Geophys Res 115, G04022. doi:10.1029/2010JG001340

Ellsworth DS, Reich PB (1993) Canopy structure and vertical patterns of photosynthesis and related leaf traits in a deciduous forest. Oecologia 96:169–178. doi:10.1007/BF00317729

Farquhar GD, von Caemmerer S, Berry JA (1980) A biochemical model of photosynthetic CO2 assimilation in leaves of C3 species. Planta 149:78–90. doi:10.1007/BF00386231

Givnish TJ (1988) Adaptation to sun and shade: a whole-plant perspective. Aust J Plant Physiol 15:63–92. doi:10.1071/PP9880063

Good SP, Rodriguez-Iturbe I, Caylor KK (2013) Analytical expressions of variability in ecosystem structure and function obtained from three dimensional stochastic vegetation modeling. Proc R Soc A 469(215520130003):1471–2946. doi:10.1098/rspa.2013.0003

Gower ST, Vogel JG, Norman JM, Kucharik CJ, Steele SJ, Stow TK (1997) Carbon distribution and aboveground net primary production in aspen, jack pine, and black spruce stands in Saskatchewan and Manitoba, Canada. J Geophys Res 102:29,029–29,041. doi:10.1029/97JD02317

Hadley JL, O'Keefe J, Munger JW, Hollinger DY, Richardson AD (2009) Phenology of forest-atmosphere carbon exchange for deciduous and coniferous forests in southern and northern New England: Variation with latitude and landscape position. In: Noormets A (ed) Phenology of ecosystem processes: applications in global change research. Springer Verlag, Dordrecht, pp 119–141. doi:10.1007/978-1-4419-0026-5_5

Harley PC, Baldocchi DD (1995) Scaling carbon dioxide and water vapour exchange from leaf to canopy in a deciduous forest. I. Leaf model parametrization. Plant Cell Environ 18:1146–1156. doi:10.1111/j.1365-3040.1995.tb00625.x

Ingestad T, Lund A-B (1986) Theory and techniques for steady state mineral nutrition and growth of plants. Scand J For Res 1:439–453. doi:10.1080/02827588609382436

Jarvis PG (1976) The interpretation of the variation in leaf water potential and stomatal conductance found in canopies in the field. Philos Trans R Soc Lond B 273:593–610

Jarvis PG (1995) Scaling processes and problems. Plant Cell Environ 18(10):1079–1089. doi:10.1111/j.1365-3040.1995.tb00620.x

Kattge J, Knorr W, Raddatz T, Wirth C (2009) Quantifying photosynthetic capacity and its relationship to leaf nitrogen content for global-scale terrestrial biosphere models. Glob Chang Biol 15:976–991. doi:10.1111/j.1365-2486.2008.01744.x

Kimball JS, Thornton PE, White MA, Running SW (1997) Simulating forest productivity and surface–atmosphere carbon exchange in the BOREAS study region. Tree Physiol 17:589–599. doi:10.1093/treephys/17.8-9.589

Kobayashi H, Baldocchi DD, Ryu Y, Chenc Q, Maa S, Osunaa JL, Ustind SL (2012) Modeling energy and carbon fluxes in a heterogeneous oak woodland: a three-dimensional approach. Agric For Meteorol 152:83–100. doi:10.1016/j.agrformet.2011.09.008

Kolic B (1978) Forest ecoclimatology (in Serbian). University of Belgrade, Belgrade, p 295

Kotchenova SY, Song X, Shabanov NV, Potter CS, Knyazikhin Y, Myneni RB (2004) Lidar remote sensing for modeling gross primary production of deciduous forests. Remote Sens Environ 92:158–172. doi:10.1016/j.rse.2004.05.010

Lalic B, Mihailovic DT (2004) An empirical relation describing leaf-area density inside the forest for environmental modeling. J Appl Meteorol 43:641–645. doi:10.1175/1520-0450(2004)043<0641:AERDLD>2.0.CO;2

Lalic B, Firanj A, Mihailovic DT, Podrascanin Z (2013) Parameterization of PAR vertical profile within horizontally uniform forest canopies for use in environmental modeling. J Geophys Res Atmos 118:8156–8165. doi:10.1002/jgrd.50626

Law BE, Cescatti A, Baldocchi DD (2001) Leaf area distribution and radiative transfer in open-canopy forests: implications for mass and energy exchange. Tree Physiol 21:777–787

Leuning R, Kelliher FM, de Pury DGG, Schulze ED (1995) Leaf nitrogen, photosynthesis, conductance and transpiration: scaling from leaves to canopy. Plant Cell Environ 18:1183–1200. doi:10.1111/j.1365-3040.1995.tb00628.x

Lloyd J, Taylor JA (1994) On the temperature dependence of soil respiration. Funct Ecol 8(3):315–323. doi:10.2307/2389824

Mahfouf JF (1990) A numerical simulation of the surface water budget during HAPEX-MOBILHY. Bound-Layer Meteorol 53(3):201–222. doi:10.1007/BF00154442

Malhi Y, Baldocchi DD, Jarvis PG (1999) The carbon balance of tropical, temperate and boreal forests. Plant Cell Environ 22:715–740. doi:10.1046/j.1365-3040.1999.00453.x

Medlyn BE, Badek F-W, de Pury DGG, Barton CVM, Broadmeadow M, Ceulemans R et al (1999) Effects of elevated [CO_2] on photosynthesis in European forest species: a meta-analysis of model parameters. Plant Cell Environ 22:1475–1495. doi:10.1046/j.1365-3040.1999.00523.x

Mercado LM, Lloyd J, Carswell F, Mahli Y, Meir P, Nobre A (2006) Modelling Amazonian forest eddy covariance data: a comparison of big leaf versus sun/shade model for the C-14 tower at Manaus I. Canopy photosynthesis. Acta Amazon 36:69–82. doi:10.1590/S0044-59672006000100009

Mihailovic DT (1996) Description of a land–air parameterization scheme (LAPS). Global Planet Chang 13:207–215. doi:10.1016/0921-8181(95)00048-8

Mihailovic DT (2003) Implementation of land-air parameterization scheme (LAPS) in a limited area model. *Final Report*. The New York State Energy Conservation and Development Authority, Albany, NY, 110 pp

Mihailovic DT, Eitzinger J (2007) Modelling temperatures of crop environment. Ecol Model 2:465–475. doi:10.1016/j.ecolmodel.2006.11.009

Mihailovic DT, Kallos G (1997) A sensitivity study of a coupled soil-vegetation boundary-layer scheme for use in atmospheric modeling. Bound-Layer Meteorol 82:283–315. doi:10.1023/A:1000169412287

Mihailovic DT, Rajkovic B, Lalic B, Dekic L (1995) Schemes for parameterizing evaporation from a non-plant-covered surface and their impact in on partitioning the surface energy in land–air exchange parameterization. J Appl Meteorol 34:2462–2475. doi:10.1175/1520-0450(1995)034<2462:SFPEFA>2.0.CO;2

Mihailovic DT, Lee TJ, Pielke RA, Lalic B, Arsenic ID, Rajkovic B (2000) Comparison of different boundary layer surface schemes using single point micrometeorological field data. Theor Appl Climatol 67:135–151. doi:10.1007/s007040070003

Mihailovic DT, Lalic B, Arsenic I, Eitzinger J, Dusanic N (2002) Simulation of air temperature inside the canopy by the LAPS surface scheme. Ecol Model 147:199–207. doi:10.1016/S0304-3800(01)00422-7

Mihailovic DT, Lazic J, Leśny J, Olejnik J, Lalic B, Kapor D, Cirisan A (2010) A new design of the LAPS land surface scheme for use over and through heterogeneous and non-heterogeneous surfaces: numerical simulations and tests. Theor Appl Climatol 100:299–323. doi:10.1007/s00704-009-0184-z

Misson L, Baldocchi DD, Black TA et al (2007) Partitioning forest carbon fluxes with overstory and understory eddy-covariance measurements: a synthesis based on FLUXNET data. Agric For Meteorol 144:14–31. doi:10.1016/j.agrformet.2007.01.006

Mix W, Goldberg V, Bernhardt KH (1994) Numerical experiments with different approaches for boundary layer modeling under large-area forest canopy conditions. Meteorol Z 3:187–192

Munger W, Wofsy S (1999) Canopy-atmosphere exchange of carbon, water and energy at Harvard Forest EMS Tower since 1991. Harvard Forest Data Archive: HF004

Newcomer J, Landis D, Conrad S, Curd S, Huemmrich K, Knapp D, Morrell A, Nickeson J, Papagno A, Rinker D, Strub R, Twine T, Hall F, Sellers P, et al (2000) Collected data of the Boreal Ecosystem-Atmosphere Study. CD-ROM. NASA

Niu S, Yuan Z, Zhang Y, Liu W, Zhang L, Huang J et al (2005) Photosynthetic responses of C3 and C4 species to seasonal water variability and competition. J Exp Bot 56:2867–2876. doi:10.1093/jxb/eri281

Norman JM (1993) Scaling processes between leaf and canopy. In: Ehleringer JR, Field C (eds), Scaling physiological processes: leaf to globe. Academic Press, pp 41–75

Pan Y, Birdsey RA, Fang J et al (2011) A large and persistent carbon sink in the world's forests. Science 333:988–993. doi:10.1126/science.1201609

Pielke PA (1984) Mesoscale meteorological modeling. Academic, New York

Schaefer K, Schwalm CR, Williams C et al (2012) A model-data comparison of gross primary productivity: results from the North American Carbon Program site synthesis. J Geophys Res 117, G03010. doi:10.1029/2012JG001960

Sellers PJ, Mintz Y, Sud YC, Dalcher A (1986) A simple biosphere model (Sib) for use within general-circulation models. J Atmos Sci 43(6):505–531. doi:10.1175/1520-0469(1986)043<0505:ASBMFU>2.0.CO;2

Sellers PJ, Dickinson RE, Randall DA et al (1997a) Modeling the exchanges of energy, water, and carbon between continents and the atmosphere. Science 275(5299):502–509. doi:10.1126/science.275.5299.502

Sellers PJ, Hall FG, Kelly RD, Black A, Baldocchi D, Berry J, Ryan M, Jon Ranson K, Crill PM, Lettenmaier DP, Margolis H, Cihlar J, Newcomer D, Goodison B, Wickland DE, Guertin FE (1997b) BOREAS in 1997: experiment overview, scientific results, and future directions. J Geophys Res 102(D4):28,731–28,769. doi:10.1029/97JD03300

Song Q, Zhang G, Zhu X-G (2012) Optimal crop canopy architecture to maximise canopy photosynthetic CO_2 uptake under elevated CO_2—a theoretical study using a mechanistic model of canopy photosynthesis. Funct Plant Biol 40:109–124. doi:10.1071/FP12056

Sprintsin M, Chen JM, Desai A, Gough CM (2012) Evaluation of leaf-to-canopy upscaling methodologies against carbon flux data in North America. J Geophys Res 117, G01023. doi:10.1029/2010JG001407

Treuhaft RN, Asner GP, Law BE, Van Tuyl S (2002) Forest leaf area density profiles from the quantitative fusion of radar and hyperspectral data. J Geophys Res 107(D21):4568. doi:10.1029/2001JD000646

Urbanski S, Barford C, Wofsy S, Kucharik C, Pyle E, Budney J, McKain K, Fitzjarrald D, Czikowsky M, Munger JW (2007) Factors controlling CO_2 exchange on timescales from hourly to decadal at Harvard Forest. J Geophys Res 112, G02020. doi:10.1029/2006JG000293

von Caemmerer S, Farquhar GD (1981) Some relationships between the biochemistry of photosynthesis and the gas exchange of leaves. Planta 153:376–387. doi:10.1007/BF00384257

Wullschleger SD (1993) Biochemical limitations to carbon assimilation in C3 plants—a retrospective analysis of the A/Ci curves from 109 species. J Exp Bot 44:907–920. doi:10.1093/jxb/44.5.907

Yuan W, Liu S, Zhou G et al (2007) Deriving a light use efficiency model from eddy covariance flux data for predicting daily gross primary production across biomes. Agric For Meteorol 143:189–207. doi:10.1016/j.agrformet.2006.12.001

Zeng P, Takahashi H (2000) A first order closure model for the wind flow within and above vegetation canopies. Agric For Meteorol 103:301–313. doi:10.1016/S0168-1923(00)00133-7